Pullout of metallic fibres from a ceramic refractory matrix

Emmanuel Cailleux, Thierry Cutard, Gérard Bernhart

Pullout of metallic fibres from a ceramic refractory matrix

E. Cailleux, T. Cutard*, G. Bernhart

Centre de Recherche Outillages, Matériaux et Procédés, Ecole des Mines d'Albi-Carmaux, route de Teillet, Albi 81000, France

Abstract

The extraction behaviour of stainless steel fibres from a ceramic refractory matrix has been studied by way of pullout tests and scanning electron microscopy observations. The effect of first heating of such composites has been characterised both by room temperature pullout tests and by dilatometric experiments. High temperature pullout tests have been performed too. Mechanical and microstructural evolutions are discussed with the help of analytical models.

Keywords: A. Ceramic matrix composites (CMCs); B. Fibre/matrix bond; B. Interface/interphase; B. High-temperature properties; D. Mechanical testing

1. Introduction

The incorporation of steel fibres in a cementitious matrix is well known to lead to an increase in the dissipated energy during structural cracking. The major effect of metallic fibres is to act as bridging ligaments in the crack plane in order to limit crack propagation and opening. In this field, several studies have shown that fibres debond or break and then pull out of the matrix by slipping in the initial geometry [1–3].

Few studies have been made on the reinforcement of ceramic refractories with metallic fibres. Higher temperature applications are targeted when compared to classical cementitious materials. As an example, they may be used as superplastic moulds in the aeronautic industry [4,5]. Working temperatures are close to 500 °C for aluminium alloys and to 900 °C for titanium alloys. Micromechanisms involved in crack bridging have to be carefully investigated in order to understand and to predict the composite behaviour. In the present paper, the pullout test has been used to characterise the extraction behaviour of a metallic fibre from a ceramic refractory matrix. More attention has been paid both to the effect of the firing temperature and the test temperature. The effect of the firing temperature has been investigated with the help of room temperature pullout tests and of scanning electron microscopy (SEM) observations. The effect of the working temperature has been studied by the way of high temperature pullout tests. In both cases, results are discussed with support of analytical models.

2. Materials and experiments

The ceramic refractory matrix consists of an inorganic alumino-silicate binder phase and of cordierite aggregates. The binder phase is obtained by mixing a solid and a liquid precursors [6]. The solid one consists of a major alumino-silicate oxide and of thermal silica fume. The liquid precursor is an aqueous solution of potassium polysilicate. Aggregates consist of a mixture of four granulometric ranges (0–125 μm, 0.2–0.5 mm; 0.5–1.5 mm; 1.5–3 mm) of a commercial cordierite grog. The ceramic refractory is shaped by mixing these different components and by casting under vibrations. Complete polymerisation of the binder phase is obtained after an isothermal heat treatment of 12 h at 80 °C. The resulting reaction product has a chemical composition close to that of the orthoclase mineral phase ($K(AlSi_3)O_8$). Previous works have shown that for applications as mould in the field of the superplastic forming process (SPF), this ceramic refractory has to be previously fired at 500 °C for aluminium parts and at 980 °C for titanium parts [5,7].

Metallic fibres are made of an AISI 310 stainless steel and are processed by cold drawing. Three diameters have been considered in the present work: 0.38, 1 and 2 mm. Pullout samples have been elaborated following the processing route of the ceramic refractory and after a fitting of the fibre in the casting mould. Cylindrical sample dimensions are 25 mm in diameter and 80 mm in length. Two fibre embedded lengths have been considered: 6 and

* Corresponding author. Tel.: +33-5-63-49-31-61; fax: +33-5-63-49-30-99.

E-mail address: cutard@enstimac.fr (T. Cutard).

Table 1
Mechanical properties of AISI310 stainless steel fibres

Firing temperature (°C)	$\sigma_{0.02}$ (MPa) at 20 °C	$\sigma_{0.02}$ (MPa) at 500 °C	E (GPa) at 20 °C	E (GPa) at 500 °C
80	560		180	
500	757	499	206	157
980	298		187	

$\sigma_{0.02}$: 0.02% yield stress; E: Young's modulus.

Table 2
Mechanical properties of ceramic refractory

Firing temperature (°C)	σ_R (MPa) at 20 °C	σ_R (MPa) at 500 °C	E (GPa) at 20 °C	E (GPa) at 500 °C
80	5.1		14.1	
500	3.2	3.6	8.2	8.1

σ_R: rupture stress; E: Young's modulus.

12 mm. With respect to the polymerisation process of the binder phase and to the application temperature of the SPF process, the 80, 500 and 980 °C firing temperatures have been retained for these pullout samples. Mechanical properties of the components after such thermal treatments have been determined by room temperature and high temperature tensile tests (Tables 1 and 2).

Pullout tests have been performed on an INSTRON 4467 device equipped with a 500 N load cell. Fig. 1 shows the pullout test in the high temperature configuration. Sample base is glued to the upper water-cooled plate. The fibre extremity is fitted in a lower tensile grip. Heating is performed by a MTS 653 furnace with two heating zones. Thermal gradient has been measured in the 12 mm area of the fibre embedded length and is less than 1 °C at 500 °C. Fibre extraction is measured with a high temperature extensometer.

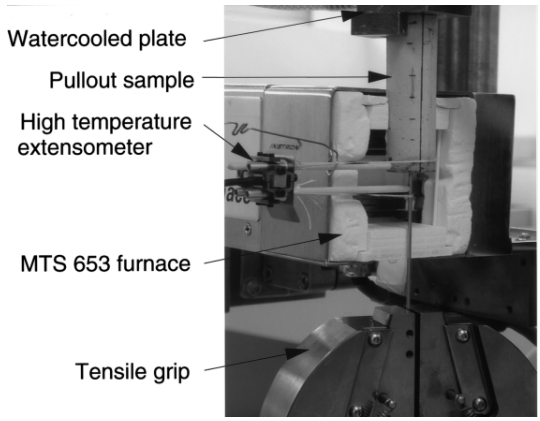

Fig. 1. High temperature pullout test (opened furnace).

3. Results and discussion

3.1. Room temperature tests

Fig. 2 shows load–displacement curves obtained for a 0.38 mm fibre diameter. The conventional domains of a pullout curve are found: in the debonding domain, these curves rise regularly up to a maximum load P_{max} and the friction domain begins after a load drop.

The firing temperature influences the pullout behaviour. In the debonding domain, the increase of this temperature leads to an evolution from a linear behaviour to a non-linear one. This indicates a transition from an instantaneous debonding mode to a progressive debonding one [8]. A decrease of the maximum load (P_{max}) at the end of the debonding domain is observed too when increasing the firing temperature. This is confirmed on the plots of Fig. 3, which show the evolution of the interfacial shear stress τ_{peak} at the end of the debonding domain as a function of the firing temperature. Each point of these plots is the average of five tests and τ_{peak} has been calculated taking into account the fibre radius r_f and the embedded fibre length L_0 as follows:

$$\tau_{peak} = \frac{P_{max}}{2\pi L_0 r_f} \quad (1)$$

Furthermore, these curves show the great influence of the fibre diameter on the shear stress. Lower values have been systematically measured when increasing this diameter.

In the friction domain, the load levels decrease both with the increase in the firing temperature and in the fibre diameter. Except for the tests performed after a 80 °C heat treatment, the friction load tends to decrease with the fibre displacement.

SEM observations have been performed on the fibre/matrix interfaces after the firing treatment. Two types of

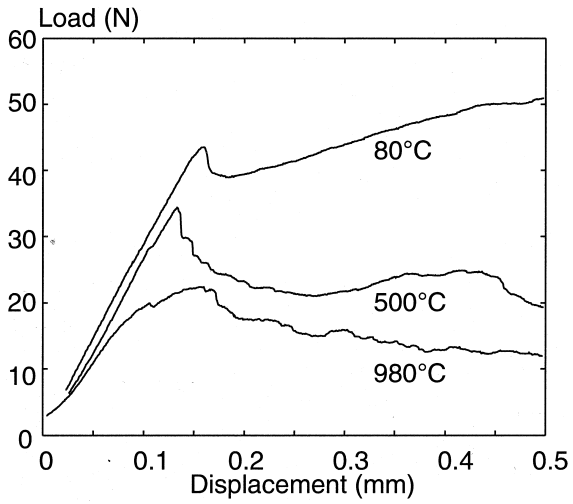

Fig. 2. Pullout curves at 20 °C for a 0.38 mm fibre diameter and for three firing temperatures.

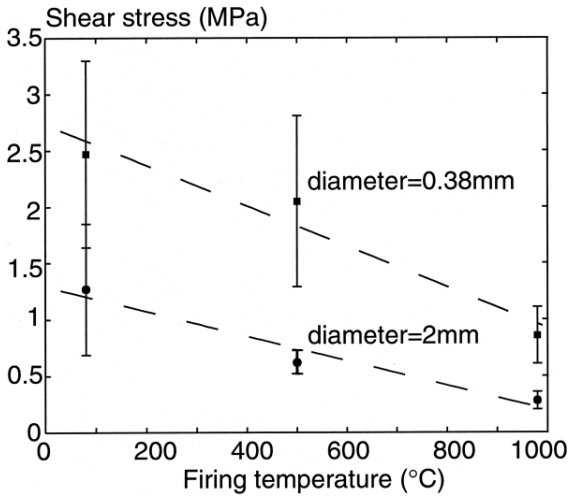

Fig. 3. Evolutions of the interfacial shear stress (τ_{peak}) as a function of the firing temperature and the fibre diameter.

transformations were observed. The first one deals with radial cracks (cf. Fig. 4(a)) and the second one with fibre/matrix debondings (cf. Fig. 4(b)). Such observations indicate that the stress fields, which developed during this first thermal cycle, have lead to a damage process in the composite microstructure.

An analytical estimation of the local stress levels induced by the heating of a microcomposite made of a fibre embedded in a cylindrical matrix block can be performed (Fig. 5). In the initial state, the microcomposite is assumed as free of internal stresses. As a result of the fibre/matrix thermal expansion mismatch and of the increase (ΔT) of the temperature, a fretting pressure P_N is developed at the interface; it can be expressed as follows

$$P_N = \frac{(\alpha_f - \alpha_m)\Delta T}{\frac{(1+\nu_m)}{E_m} + \frac{(1-\nu_f)}{E_f}} \tag{2}$$

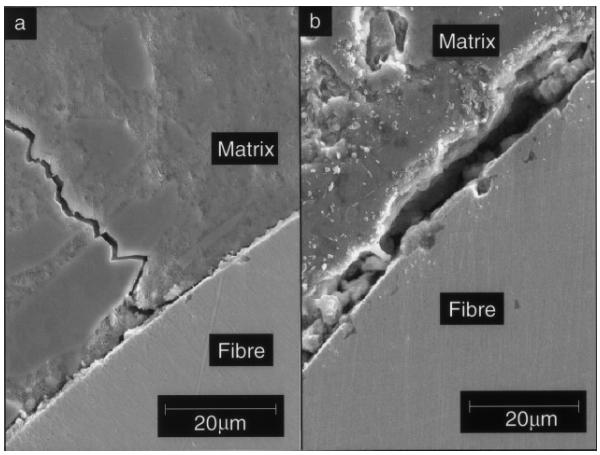

Fig. 4. SEM micrographs of fibre/matrix interfaces after a 500 °C firing treatment.

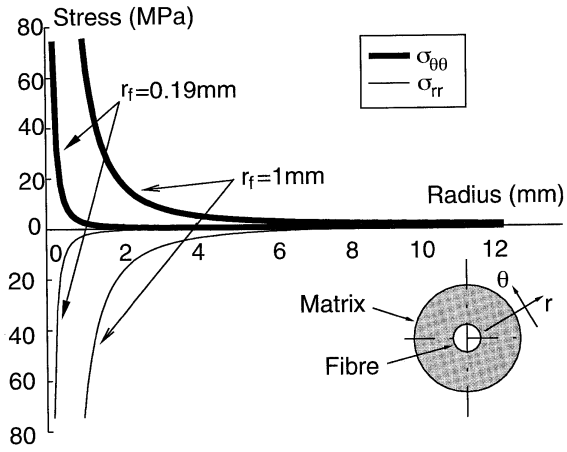

Fig. 5. Stress levels induced in the matrix by the heating of the microcomposite from 20 °C to 500 °C.

where α_i, ν_i and E_i are, respectively, the thermal expansion coefficient, the Poisson ratio and the Young's modulus of the component i (i = f for the fibre and i = m for the matrix).

The stress levels in the matrix shell can be expressed as a function of this fretting pressure using classical linear elasticity equations [9]. Evolutions of the radial stress σ_{rr} and of the tangential stress $\sigma_{\theta\theta}$ as a function of the radius r in the matrix can be expressed as follows

$$\sigma_{rr} = \frac{P_N r_f^2}{r_m^2 - r_f^2}\left(1 - \frac{r_f^2}{r}\right) \quad \text{and} \qquad \sigma_{\theta\theta} = \frac{P_N r_f^2}{r_m^2 - r_f^2}\left(1 + \frac{r_f^2}{r}\right) \tag{3}$$

where r_m is the external radius of the matrix cylinder.

From these expressions and from the properties listed in Table 3, the evolutions of the radial and tangential stress can be plotted as a function of the radius. Fig. 5 shows such a plot for a temperature increase from 20 to 500 °C (ΔT = 480 °C). Tangential stresses clearly exceed the rupture stress of the matrix at 500 °C, which is reported in Table 1. The 76 MPa tensile stress level calculated at the fibre/matrix interface is much than the rupture stress value of 3.6 MPa determined by tensile tests [7]. Such high stress levels can clearly be responsible for the radial matrix cracking, which is observed after the first thermal cycle.

Table 3
Properties of the fibre and of the matrix at 500 °C

Property	Matrix	Fibre
Young's modulus (GPa)	8.1	157
Poisson ratio	0.2	0.3
Thermal expansion coefficient (10^{-6} K^{-1})	−6[a]	17.8

[a] This negative value indicates the shrinkage, which occurs in the ceramic refractory matrix during the first heating and which was measured by dilatometry.

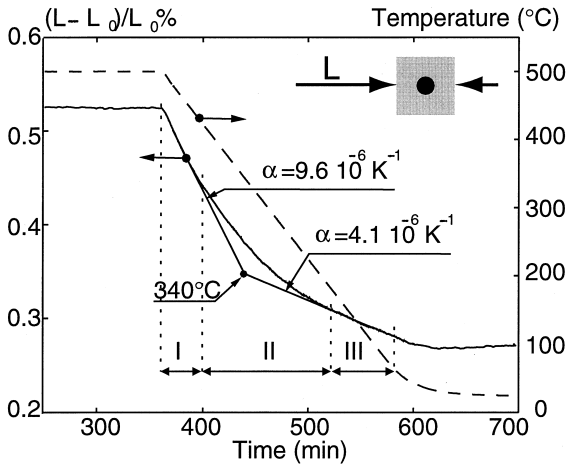

Fig. 6. Dilatometric behaviour of a microcomposite during the first cooling between 500 and 20 °C. The continuous line indicate the dilatometric evolutions as a function of time and the doted line the evolutions of the temperature as a function of time.

The compressive radial stress levels are rather high too. They may influence both the fibre expansion and the matrix shrinkage at high temperature. This gives an explanation of the fibre/matrix debonding that have been previously observed. This hypothesis is confirmed by the results of transversal dilatometric tests performed on microcomposites. The geometry of such a sample and an example of these results are presented in Fig. 6.

During the first cooling of such a microcomposite, a non-linear dilatometric behaviour is observed. At the beginning of the cooling, a first linear domain (domain I) is observed from a $9.6 \times 10^{-6}\,K^{-1}$ thermal expansion coefficient (α). This is an intermediate value between the thermal expansion of the stainless steel fibre ($17.8 \times 10^{-6}\,K^{-1}$) and the thermal expansion of the ceramic refractory matrix, which is of $4.2 \times 10^{-6}\,K^{-1}$ after a 500 °C firing. At the end of the cooling, another linear domain (domain III) is observed and leads to a thermal expansion coefficient of $4.1 \times 10^{-6}\,K^{-1}$. This value is equal to the ceramic refractory one. In an intermediate domain (domain II), centred on a 340 °C temperature, a progressive transition from the linear behaviour of domain I to the one of domain III is observed. This indicates the existence of a contact between the fibre and the matrix at high temperature. In this case, both components contribute to the dilatometric behaviour of the microcomposite At lower temperatures (in domain II), a fibre/matrix decohesion starts to appear and in domain III, the ceramic refractory is only involved in the dilatometric behaviour of the microcomposite. The reversibility of this dilatometric behaviour has been measured with a second thermal cycle. During the second heating, the 340 °C transition temperature (T_T) is confirmed. At this temperature, a recovery of the fibre/matrix contact is obtained.

SEM observations have been performed on the fibre surfaces after room temperature pullout tests. In the case of 500 or 980 °C fired samples, numerous adhesion areas of ceramic refractory are observed on the fibre surface (Fig. 7(a)) as previously seen in other brittle matrix composites [10,11]. Such matrix adhesion areas may lead to an increase in the load level required to extract the fibre. It explains that non-zero loadings are necessary to extract fibres from the ceramic refractory matrix even if interfacial debondings are observed. If R is the thickness of these adhesion areas and δ_d the debonding distance between the fibre and the matrix after the firing treatment, the pullout of the fibre requires an imposed radial displacement of the fibre/matrix interface of $R - \delta_d$. At room temperature, such a mechanism induces a fretting pressure P'_N which can be calculated as follows [7]:

$$P'_N = \frac{\dfrac{(R-\delta_d)}{r_f}}{\dfrac{(1+\nu_m)}{E_m} + \dfrac{(1-\nu_f)}{E_f}} \tag{4}$$

with

$$\delta_d = (\alpha_f - \alpha_m)(T_T - T_a)r_f \tag{5}$$

where T_T is the transition temperature and T_a the room temperature.

Considering a Coulomb friction model, the shear stress τ_f, which becomes necessary to extract the fibre is equal to:

$$\tau_f = \mu P'_N \tag{6}$$

where μ is the friction coefficient.

From Eqs. (4)–(6), it can be seen that an increase in the fibre radius will lead to an increase in the debonding distance δ_d and therefore to a decrease of P'_N and τ_f. This is in good agreement with the decrease of τ_f which has been measured when increasing the fibre diameter.

In the case of 80 °C fired samples, SEM observations of the fibre surfaces clearly indicate the existence of abrasion mechanisms during the pullout process (cf. Fig. 7(b)). Matrix particles are often included in the fibres. In such cases, large plastic deformation fields are observed. Such mechanisms can explain the increase in the pullout load

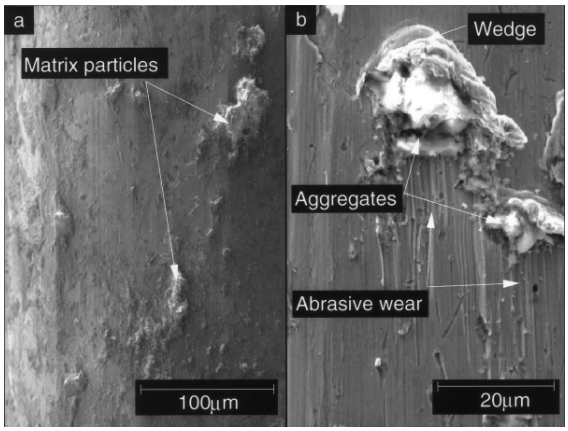

Fig. 7. SEM micrographs of the fibre surface after pullout tests on samples previously fired: (a) at 500 °C (b) at 80 °C.

observed with displacement even if the embedded fibre length decreases (cf. Fig. 2).

3.2. High temperature tests

Fig. 8 gives an example of a pullout test performed at high temperature. In this case, two similar samples were fired at 500 °C during the same heat treatment. The first one was tested at 20 °C and the second one at 500 °C. Increasing the test temperature has led to two major evolutions in the extraction behaviour.

The first one deals with the higher load levels which are measured both in the debonding and friction domains compared to the 20 °C test. Such a behaviour is of great interest for high temperature applications of composites based on the association of these two components. As a result of the temperature increase, a fretting pressure develops at the interface and a supplementary loading has to be applied to extract the fibre from the matrix. As previously proposed by Pinchin and Tabor the extraction load F_{extr} after the debonding peak may be divided into two components [12]. The first one (F_1) corresponds to the necessary load to extract a fibre in contact with the matrix without any fretting pressure. In the present work, the extraction of a fibre from a 80 °C fired sample corresponds to such a case. The second component (F_2) takes into account the fretting pressure at the test temperature (T_{test}) and the radial fibre contraction due to the Poisson effect [12]:

$$F_2 = \left(1 - \exp\left(\frac{-2\nu_f \mu L_0}{E_f r_f\left(\frac{1+\nu_m}{E_m} + \frac{1-\nu_f}{E_f}\right)}\right)\right) \times \frac{(\alpha_f - \alpha_m)(T_{test} - T_T)E_f \pi r_f^2}{\nu_f} \quad (7)$$

where L_0 is the embedded fibre length.

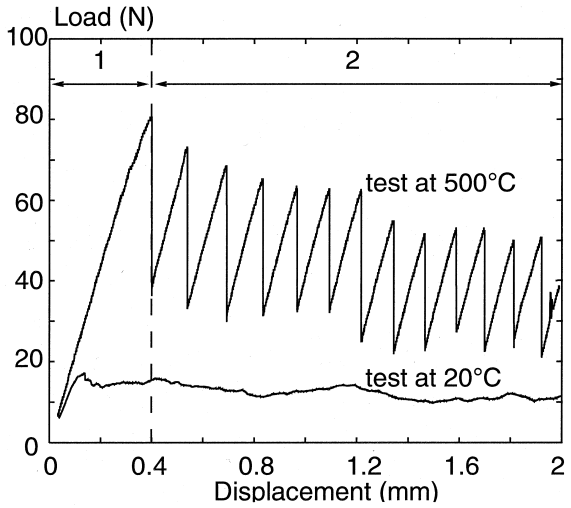

Fig. 8. Pullout curves of 0.38 mm in diameter fibres after a 500 °C firing treatment and for 20 and 500 °C test temperatures.

Table 4
Comparison between experimental and calculated values of the extraction load F_{extr} for a 0.38 mm fibre diameter and a 500 °C test temperature

L_0 (mm)	F_1 (N) (experiment)	F_2 (N) (calculated)	F_{extr} (N) (experiment)	F_{extr} (N) (calculated)
6	23	21	52	44
12	35	41	74	76

Table 4 gives a comparison between the experimental and calculated values of F_{extr} in the case of a 0.38 mm fibre diameter and for a 500 °C test temperature (with $F_{extr} = F_1 + F_2$). The friction coefficient is assumed to be equal to 0.2, a consistent value for a sliding contact between metallic and ceramic bodies [13].

The second evolution due to the increase of the test temperature involves the emergence of a stick slip mode. Previous works have established the origin of such a stick slip behaviour in sliding experiments [14,15]. In the present case, three parameters can be considered as responsible for this mechanism: the fretting pressure, the system stiffness, and the extraction velocity. The only parameters which follow an important evolution between room temperature and high temperature tests is the fretting pressure. This pressure can be considered as responsible for this evolution from a steady sliding behaviour at 20 °C to a stick slip one at 500 °C.

4. Conclusion

In this study, a steel fibre reinforced ceramic refractory has been characterised using pullout tests and SEM observations of fibre/matrix interfaces. Results show the great influence of the manufacturing temperature history on the mechanical behaviour.

During the first thermal cycle, large stress levels appear near the fibre/matrix interface as a consequence of the thermal expansion mismatch between the two components. As a result of such stress fields, a damage process is initiated in terms of radial matrix cracking and of fibre/matrix decohesion. This last mechanism occurs during the cooling of the first thermal cycle and at a transition temperature, which depends on the maximum temperature of the cycle. It leads to a decrease of the fibre pullout load level at room temperature. The reversibility of this decohesion process leads to an important increase of the pullout performance during high temperature tests. This is mainly due to the development of a fretting pressure at the fibre/matrix interface. Such a behaviour is of great interest for high temperature applications of composites based on these two components. This is particularly true to limit the brittle behaviour that characterises unreinforced ceramic refractories.

Further works are in progress to investigate and quantify the effect of the fibre orientation with the load axis. In a second way, studies of the macro mechanical properties of

composites based on this fibre/matrix association were started. Links between the micromechanic and the macro mechanic scales will then be performed.

References

[1] Naaman AE, Shah SP. Pull-out mechanism in steel fiber-reinforced concrete. J Struct Div, Proc ASCE 1976;102(8):1537–49.

[2] Bartos P. Bond in fibre reinforced cements and concretes. Int J Cement Compos Lightweight Concrete 1981;3(3):1–18.

[3] Chanvillard G. Modelling of wiredrawn steel fibres debonding. Proceedings of BMC4 Conference, Warsaw; September 1994. p. 311–9.

[4] Yaofu G, Naicheng G, Daren Z, Mancai H. The superplastic forming of metal sheets using a die of refractory concrete. J Mater Process Technol 1992;30:159–66.

[5] Cutard T, Cailleux E, Lours P, Bernhart G. Structural and mechanical properties of a refractory concrete for superplastic forming tools. Ind Ceram 1999;19(2):100–2.

[6] Davidovits J. Chemistry of geopolymeric systems terminology. Proceedings of Geopolymer'99 Conference, Saint Quentin; June 1999. p. 9–39.

[7] Cailleux E. Microstructure et comportement thermomécanique d'un béton réfractaire reinforcé par des fibres métalliques. PhD Thesis. Ecole des Mines de Paris; 2001. p. 241.

[8] Kerans RJ, Parthasarathy TA. Theorical analysis of the fiber pullout and pushout tests. J Am Ceram Soc 1991;74:1585–96.

[9] Timoshenko SP. Résistance des Matériaux, Dunod; 1990. p. 465.

[10] Carter WC, Butler EP, Fuller ER. Micro-mechanical aspects of asperity-controlled friction in fiber-toughened ceramic composites. Scripta Metall Mater 1991;25:579–84.

[11] Geng Y, Leung KY. A microstructural study of fibre/mortar interfaces during fibre debonding and pull-out. J Mater Sci 1996; 31:1285–94.

[12] Pinchin DJ, Tabor D. Inelastic behaviour in steel wire pull-out from Portland cement mortar. J Mater Sci 1978;13:1261–6.

[13] Guilmard Y. Mécanismes d'usure et seuils de dégradation d'une alumine en frottement contre différents alliages métalliques et cermets. PhD Thesis. Institut National Polytechnique de Toulouse; 1991. p. 232.

[14] Baumberger T, Caroli C, Perrin B, Ronsin O. Nonlinear analysis of the stick-slip bifurcation in the creep-controlled regime of dry friction. Phys Rev E 1995;51:4005–10.

[15] Baumberger T, Heslot F, Perrin B. Crossover from creep to inertial motion in friction dynamics. Lett Nature 1994;367:544–6.